



Surface modification of lotus-type porous copper by aluminization

Chuanyu Cui^{1,2} · Hao Du¹ · Jiqiang Wang¹ · Yin Yang¹ · Tianying Xiong¹

© Springer Nature Switzerland AG 2018

Abstract

This paper explores the feasibility to aluminize lotus-type porous copper to prolong the service life of lotus-type porous copper in applications. To achieve this goal, smaller particles of α -Al₂O₃, Al and NH₄Cl were employed for aluminization process considering the difficulty arising from shielding effect by pore walls. The structure of the aluminized coating including thickness, elements profile and phase composition was characterized. It is found that the deposition of aluminized coating on pore walls of the lotus-type porous copper is feasible. It is indicated that the pore size has to be more than 300 μ m in order to obtain a decent aluminized coating on pore walls of the lotus-type porous copper under the present experimental conditions. The coating is consisted of an alloy layer (first α -Cu, then a mixture of Cu₃Al and Cu₉Al₄) and a re-solidified layer (α -Al₂O₃ particles incorporated in Al substrate). Furthermore, Vickers hardness, sliding property and wear resistance were evaluated. The hardness is enhanced by a factor of three, which is distributed from 105 to 302 HV_{0.01} from copper substrate to the coating surface. It is also proved that the aluminized coating can significantly reduce the wear rate of the lotus-type porous copper by shifting the wear mechanism from adhesive mode to plowing mode by the improved hardness.

Keywords Lotus-type porous copper · Surface modification · Aluminization · Wear resistance

1 Introduction

Lotus-type porous metals with elongated directional pores fabricated by mold casting technique have been studied for decades for their superior physical and mechanical properties. These metals can be tailored to achieve controllable porosity, pore size, pore growth direction and uniform distribution of pores, as well as high specific strength and stiffness [17]. Therefore, this porous metal finds many applications to serve as both functional and structural materials, including heat sink [19], vibration-damping material [23], lubricating material [10], tissue material [2, 13], and so on. The porous metal with uniform pore size and porosity has been achieved on the metals with high thermal conductivity such as copper. However, in the case of metals especially alloys with low thermal conductivity, porous metals with uniform pore size and porosity could

not be fabricated due to poor solidification velocity of the melt. Although, new methods such as continuous zone melting technique and continuous casting technique were developed by Nakajima [17] to resolve these issues. Yet, pore size and porosity distribution are still not as uniform as pure metals with high thermal conductivity by the mold casting technique.

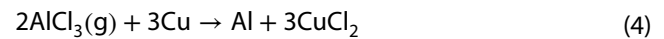
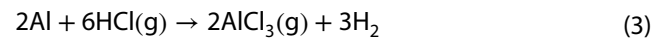
Copper is the most popular material for lotus-type structure with some beneficial properties like high thermal conductivity and high strength, which make it favorable and promising for filtration and thermal industry [7, 8, 19, 24]. However, this metal has relatively lower hardness and is prone to adhesive and abrasive wear when used for filtration and separation purpose. In addition, it has some unfavorable characteristics like surface oxidation [20] and corrosion. One feasible way to improve the wear resistance of Cu is to incorporate a hard metal in the

✉ Hao Du, hdu@imr.ac.cn | ¹Institute of Metal Research, Chinese Academy of Sciences, 72 Wenhua Road, Shenyang 110016, People's Republic of China. ²School of Materials Science and Engineering, University of Science and Technology of China, 72 Wenhua Road, Shenyang 110016, People's Republic of China.

Cu matrix so as to increase the hardness [18]. However, the presence of some additional doped elements in solid solution may reduce the electrical conductivity of the copper alloys [15]. Surface modification offers another route for improvement on those properties [18], as wear and corrosion in metals are mainly controlled by the surface properties of the material [3]. One widely used approach to tailor and improve properties of metal is to coat it with another material that exhibits superior properties [1, 2, 4, 11, 12, 14]. In the case of porous metals, the pore structure presents certain degree of difficulty to modify the surface due to the shielding effect from pore walls. Liu et al. [16] used the micro-arc oxidation method to deposit Al_2O_3 coating on open-cell Al foam. Their results showed that the coating was composed of a dense internal layer and a porous external layer. This particular structure improved the corrosion resistance of the open-cell Al foam. Wei et al. [22] aluminized porous stainless steel to achieve an intermediate layer which further facilitated the deposition of palladium membranes.

In the case of lotus-type porous metals, many researchers have put their efforts to mitigate the problem with the purpose to improve the desired properties. Nakajima et al. [1] deposited zinc on lotus-type porous copper by vaporization and diffusing the zinc into copper matrix via annealing to form a brass layer. Li et al. [12] deposited zinc layers on lotus-type porous copper by electroless plating and heat treated the samples to form a brass layer too. It can be predicted that the corrosion resistance of the coated lotus-type porous copper would be improved in both Nakajima's and Li's works. Du et al. [11] deposited nickel on the lotus-type porous copper by electroplating method which resulted in an improvement on both compression strength and absorbing energy capacity for the porous copper. Ikeda and Nakajima [14] deposited a titanium film by vapor deposition on lotus-type porous stainless steel SUS304L for a better biocompatibility. These studies have proven that the surface of lotus-type porous metals can be modified by different surface treatments to serve different purposes. However, all the coatings mentioned above are at the scale of 10 μm in thickness. In real working environment, coatings with thickness at the scale of 100 μm are more favorable for providing wear, oxidation and corrosion resistance.

Aluminization, which is relatively simple and suitable for coating a substrate with a complex geometry, can be used to form intermetallic coatings by diffusing aluminum into the metal substrate. It has been reported to be an appealing surface modification method for copper [6, 21]. In this process, the copper component is embedded in a powder mixture containing aluminum, inert Al_2O_3 filler and ammonium halide activators. The reactions can be expressed as below:



It is the gaseous AlCl_3 that reacts with Cu to deposit Al on Cu substrate. So, it may be very well applicable to lotus-type porous copper as the process is essentially a high-temperature chemical vapor deposition (CVD) process whereby AlCl_3 vapors can gain access into the inner walls of the porous copper. In addition, little impact on the pore size was found on the porous stainless steel with smaller pores by the same process in Wei et al.'s work [22]. To date, most of the reports on intermetallic compound coatings on copper surface are mainly focused on oxidation resistance improvement [21]. To the best of our knowledge, little information is available on surface modification of lotus-type porous metals via aluminization process.

In this work, possibility of applying aluminization process on lotus-type porous structure (metals) has been explored. The process was carried out on a lotus-type porous copper with an attention on pore walls. The structure of intermetallic coating on the pore walls of the porous copper was characterized, including cross-section, thickness, composition and phase structures. Furthermore, mechanical properties of the aluminized lotus-type porous copper including Vickers hardness, sliding property and wear rate were evaluated. Finally, wear mechanism was discussed for the aluminized lotus-type porous copper.

2 Experimental procedures

2.1 Aluminization process

A lotus-type porous copper with elongate pores (porosity of 48.3% and average pore size of 575 μm) was fabricated by a vacuum-assisted and pressurized casting apparatus. The details of this process were described elsewhere [9]. The ingot was then cut into rings with inner diameter of 38 mm, outer diameter of 54 mm and thickness of 5 mm. The specimens were first degreased in acetone with ultrasonic vibration for 10 min, then etched in 5% HNO_3 solution for 5 s, and rinsed with deionized water and alcohol for immediate aluminization process. The powder for the process was made of 78 wt.% Al_2O_3 , 20 wt.% Al and 2 wt.% NH_4Cl , whose morphology is shown in Fig. 1.

With the purpose to aluminize the pore walls inside the pores, the powder used in this process is relatively small. The Al_2O_3 particles are irregular cubic in shape and 10 μm in size, and the Al particles are spherical in shape

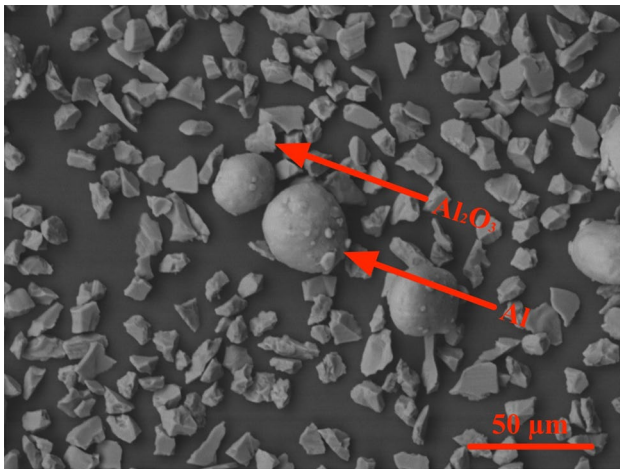


Fig. 1 The SEM image of the Al–Al₂O₃ powder used for aluminization process

and 30 μm in diameter. The powders were well mixed by a ball mill for 1 h for the next step. To perform the aluminization process, the specimens were sunk in the powders in a sealed glass tube filled by Ar gas in 1 atm., then heated to 800 $^{\circ}\text{C}$ at a rate of 10 $^{\circ}\text{C}/\text{min}$ with a holding time for 3 h in a muffle furnace. The specimens were fetched out after furnace cooling to less than 100 $^{\circ}\text{C}$ at its natural rate, and then cleaned with deionized water and alcohol to remove any residual powders.

2.2 Characterization

The specimens were first cut into 5 mm \times 5 mm \times 5 mm using an electric discharge machine (DK7763, Longhao Digital-Controlled Machine Corp., China), then degreased and rinsed using the same method described above. Prior to etching in an alcohol solution with 0.2 mol/L FeCl₃ and 0.2 mol/L HCl for 30 s, specimens were grinded by SiC papers from grit 400# to 1000#. The etched specimens were observed by an optical microscope (OM; MEF4A, Leica Microsystems, German). Pores with different sizes were cut along the growth direction and observed by the OM to determine the coating thickness along the pores. An X-ray diffractometer (XRD; D8 Discover, Bruker AXS, Germany) operating with Cu K α ($\lambda = 0.154056$ nm) radiation was used to analyze the phase structure of the coating, in which the scanning was performed on the surface and different layer on the cross-section of the coating, respectively. The diffraction angle 2θ ranged from 10 $^{\circ}$ to 90 $^{\circ}$ by a step of 0.04 $^{\circ}$. Meanwhile, the coatings were observed by a scanning electron microscope (SEM; JSM-6301F, JEOL, Japan) on cross section, while the elements distribution of the coatings was profiled by EDS (EDS; INCA L300QI, Oxford Instruments, United Kingdom). The relationship

between the pore size and the coating thickness was also measured.

2.3 Evaluation on hardness, sliding property and wear rate

The hardness of the coating was evaluated by a microhardness tester with a Vickers indenter (AKASHI MVK-EIII, Japan) under a load of 10 g and dwelling time of 15 s at 10 points on the cross section along coating thickness. Each indentation was taken no less than five times across the diagonal length and away from the other indentations to exclude stress field effect. Tribo-tests were carried out on a vertical universal friction–abrasion testing machine (MMW-1A, Jinan Yihua Tribology Testing Technology Company Ltd., China). The ring-on-ring configuration was used for the tribo-tests with carbon-steel as mating material with the size of inner diameter of 42 mm and outer diameter of 50 mm. This configuration was chosen to be sure that the size of the mating material could cover the pores. The copper rings, both the original and the aluminized, were fixed on the test machine. Before the tests, the surface layers of all the specimens were removed by grade 1200 SiC papers to be in complete contact with the counter-face. The sliding speed was set to be 157 mm/s and the loads were set to be 20 N and 50 N, respectively. The coefficient of friction was recorded by a computer connected to the machine. Wear rate was evaluated by the weight-loss method by Eq. (5):

$$W = \Delta m / \rho SF \quad (5)$$

where W is the wear rate, Δ is the weight loss after tribo-test, ρ is the density of the specimen, S is the sliding distance, F is the load. The specimens were weighted by an analytical balance (XS105, Mettler Toledo, Switzerland) with a resolution of 0.01 mg before and after the tribo-tests. The relative humidity was in the range of 50% during the tests. After the tests, the worn surfaces of the specimens were observed by SEM.

3 Results and discussion

3.1 Structure of the aluminized coating

Figure 2a shows the structure of the cross-section of the coating formed by aluminization process on the pore walls. It can be seen that the coating consists of two parts labeled as layer A and layer B with a boundary separating them. From the pore wall (copper substrate), layer A with thickness of 150 μm connects firmly with the copper substrate, layer B with thickness of 50 μm is on the layer A distributed with black particles in size of 10 μm . To

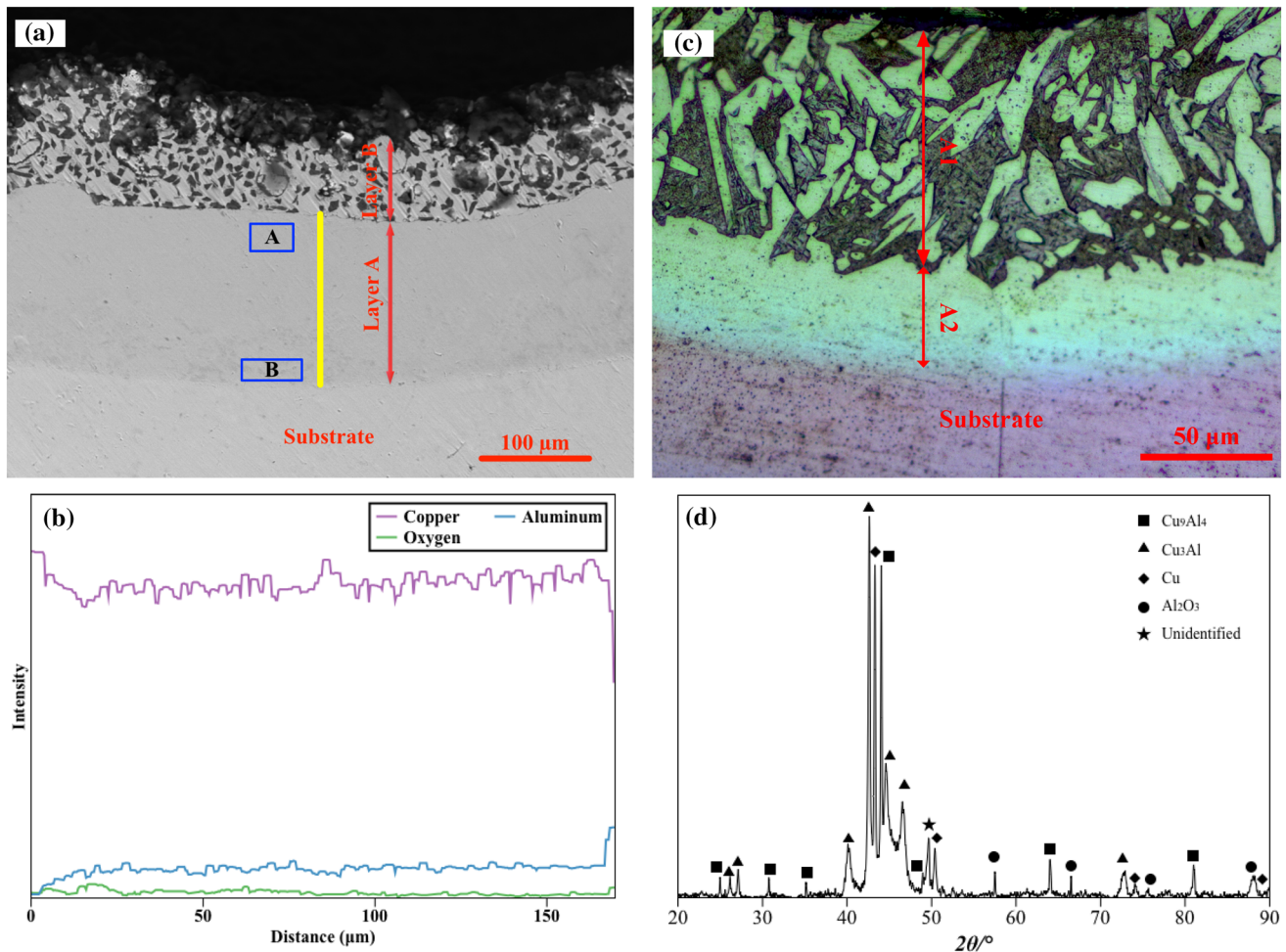


Fig. 2 The structure of the cross-section of the coating: **a** the SEM image of the whole cross-section of the coating; **b** the OM image of the cross-section of the coating after etching; **c** the EDS line-scanning of the alloy layer; **d** the XRD analysis of the cross-section of the coating

verify this point, EDS line-scan was taken along the yellow line of the layer A in Fig. 2a further. It can be found that the intensity of Al rises steadily from substrate to coating interface to the distance of 20 μm then remains at the same level despite of minor fluctuations, as shown in Fig. 2b. The intensity of Al gains a sudden rise at the end where the EDS scan exceeds the alloy layer interface to layer B. On the other hand, the intensity of Cu shows the opposite trend. It falls during the first 20 μm, then remains steady with a sudden fall at the end. The oxygen remains at a very low level throughout the whole coating. From the elements profile, it is indicated that the layer A can be further divided into two parts: the first part is about 20 μm in thickness and labeled as A2 where the proportion of Al increases steadily, and the rest is labeled as A1 where the proportion of Al remains constant. This is confirmed by OM image of the cross-section of the coating after etching (Fig. 2c). In the OM image, the thicknesses of layer A1 and layer A2 are in accordance with the element profile

shown in Fig. 2b. The XRD pattern on the cross-section of the coating is shown in Fig. 2d. The XRD results combined with EDS results (Table 1), confirm that Layer A1 may be a copper solid solution aluminum phase (α-Cu), while Layer A2 is made of Cu₃Al and Cu₉Al₄.

The layer B was further characterized, and the results are shown in Fig. 3a. It is indicated that the shape of the black particles in this layer resembles a quadrangle with an

Table 1 The EDS analysis of elements composition of different spots marked in Figs. 3a and 4b

Test points	Chemical compositions (at.%)				Possible phase
	Cu	Al	O	C	
A	71.09	21.99	5.71	1.21	Cu ₃ Al + Cu ₉ Al ₄
B	78.40	10.78	8.36	2.46	α-Cu
C	19.71	71.09	8.73	0.48	Al
D	11.78	30.70	53.13	4.39	α-Al ₂ O ₃

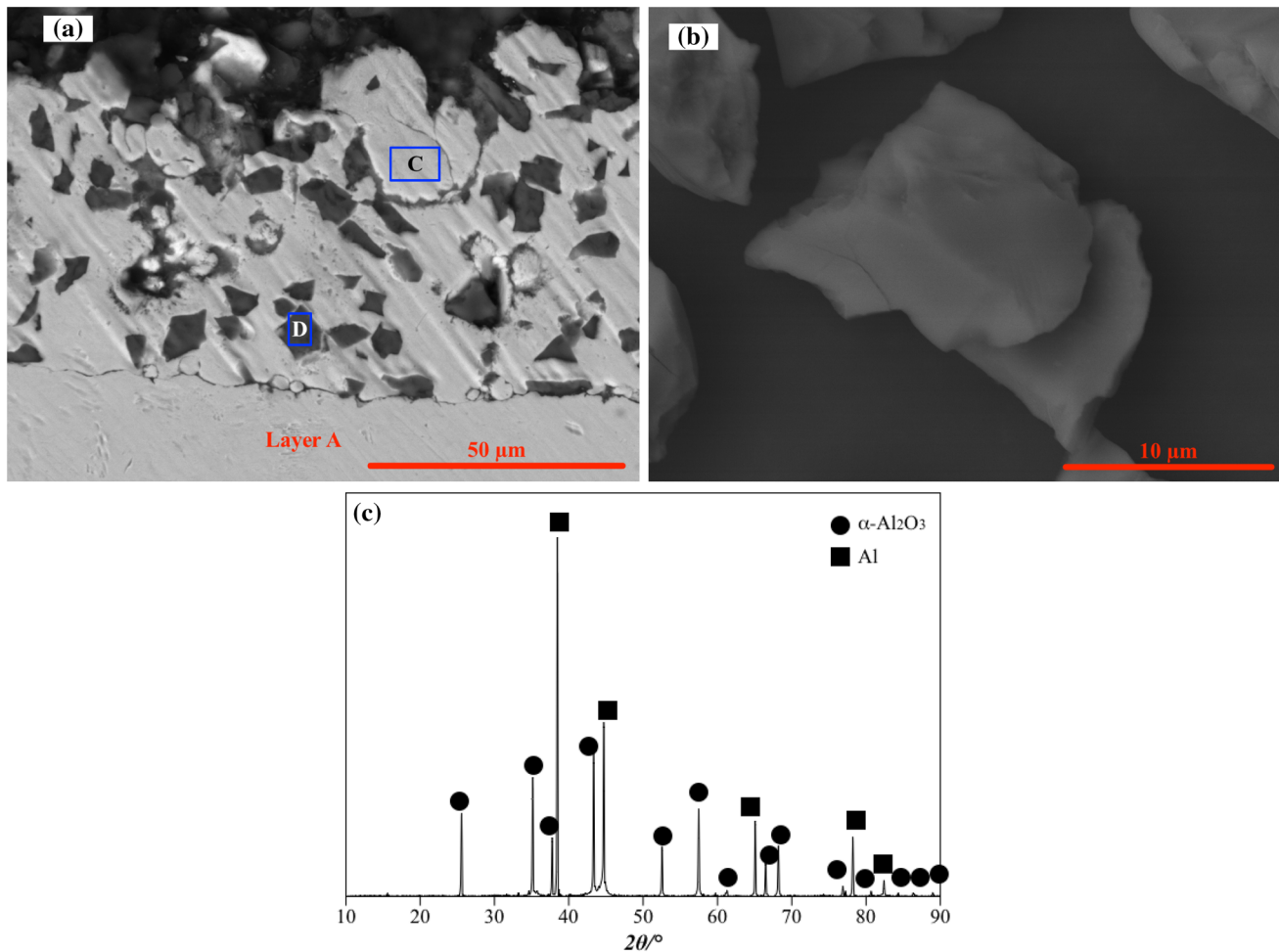


Fig. 3 The structure of the sintered layer of the coating; **a** the SEM image of sintered layer; **b** the EDS line-scanning of the sintered layer; **c** the Al₂O₃ particle used for the aluminizing process

average size of 20 μm in diagonal. This shape is the same as the starting Al₂O₃ powders used for the aluminization process, as shown in the magnified figure (Fig. 3b). Figure 3c is the XRD result of this layer. It is indicated that the layer B is made of Al and Al₂O₃. In addition, the EDS analysis on the blue spots (Table 1) shows that the black particle has 30.7 mol% Oxygen and 53.13 mol% Al while the coating has 71.09 mol% Al, 8.73 mol% oxygen. Combining all these SEM-EDS and XRD results, it is confirmed that the layer B can be regarded as a composite with Al as the substrate and the black particles Al₂O₃ as the addition phase incorporated in the substrate. As the temperature of the aluminization process in our research is 800 °C, well exceeding the melting point of Al (660.3 °C), the formation of layer B is attributed to the molten Al incorporating Al₂O₃ particles.

After the aluminization process, it is exciting to find that the porosity of the lotus-type porous copper decreased from 48.3 to 42.6% based on the weight gains, which is

much lower than the predicted value (22.9%) considering the ratio of coating thickness (150 μm) and average pore size (575 μm). This big gap on the porosity between the experimental and the predicted values may be caused by the fact that Al diffuses into the substrate and Cu also diffuses out to the coating, which will be investigated in our further work.

3.2 Effect of pore size on aluminized coating thickness

The cross section of the aluminized lotus-type porous copper is shown in Fig. 4a. It is apparent that the thickness of the aluminized coating on pore walls is much lower than that on surface, which can be understood from the nature of the deposition process as mass transport governing the deposition distribution is controlled by the pore walls. Furthermore, the thickness of the aluminized coating on pore walls differs with the pore size, the larger the

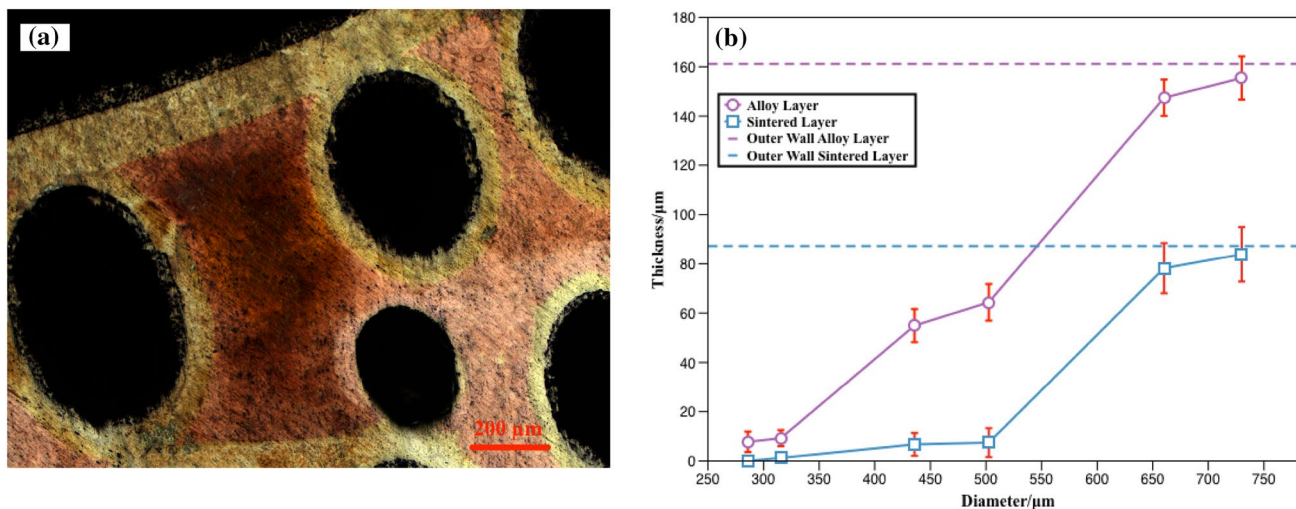


Fig. 4 Coating thicknesses on different sizes of pores: **a** OM image of the coatings on different sizes of pores; **b** Coating thickness distribution versus pore diameter diagram

pore, the thicker the coating on the pore walls. It should be mentioned that coating was not achieved on walls of some very small pores at our experimental conditions. It is accepted that in the aluminization process, the Al metal powders at the treatment temperature react with the HCl vapors produced from dissociation of the activator (NH_4Cl), resulting in the formation of precursor vapors of aluminum chlorides, which would pass and reach the pore walls. The mechanism of the aluminum deposition is mainly transferred by the disproportionate amount of lower valence chlorides at the substrate surface, followed by the subsequent solid-state inward diffusion of aluminum and outward diffusion of copper [5]. Theoretically, the thickness of the aluminized coating not only on surface but also on pore walls of the lotus-type porous metals should depend on pressure generated by the reaction, which is controlled by the amounts of the reaction powders. There should be no much difference on the thickness of the aluminized coating on pore walls of the porous metals with both large pores and small pores. However, the aluminization was carried out in a sealed glass tube with a poor pressure bearing capacity under the present experimental conditions, which limited the amount of the reaction powders. Thus, aluminium coating was formed on pore walls of the sample with large pores for the easy infiltration of the reaction gas into the pores, while a thin or even no coating was formed on the samples with small pores.

By the images, the relationship between the pore size and the coating thickness is counted and shown in Fig. 4b. It can be found that the pore size has significant impact on the coating thickness: the coating thickness is very low when the pore diameter is under 350 μm;

then, increases rapidly after the pore diameter reaches 450 μm, on both alloy layer and sintered layer; finally, remains nearly the same as that of the surface of the sample when the pore diameter is larger than 700 μm. In the case of the pores larger than 650 μm, it is interesting to find that the coating thickness starts to distribute uniformly along the pores. It is predicted that the aluminization process may be also achieved on the pores with diameter under 350 μm as well as coating uniformity when a pressurized container could be employed.

The coating morphologies along the pore growth direction are shown in Fig. 5. It is apparent that the coating thickness is not entirely the same along the pores. The thickness of the coating on the pore wall near the surface is the same as that on the surface, as shown in Fig. 5a. When the coating is located in the middle of this pore, the thickness is smaller compared with that of the coating near the surface, but more uniform, as shown in Fig. 5b, c. Deeper into the pore where the coating is located in the near bottom area, the coating grows thicker again as that in Fig. 5a. The reason behind the thickness variation is that the reactions in the near surface area are more intense. There are reactions too in the middle of the pores, which further proves that the aluminization process on lotus-type porous copper are suitable. On the other hand, the coating on the bottom of the closed pores shows a very different morphology as shown in Fig. 5e. The sintered layer piles up at the bottom and the alloyed layer is thicker than the coating on the pore wall, which is attributed to higher concentration of AlCl_3 gas at the bottom of the pores, which causes more intense reaction (reaction 4).

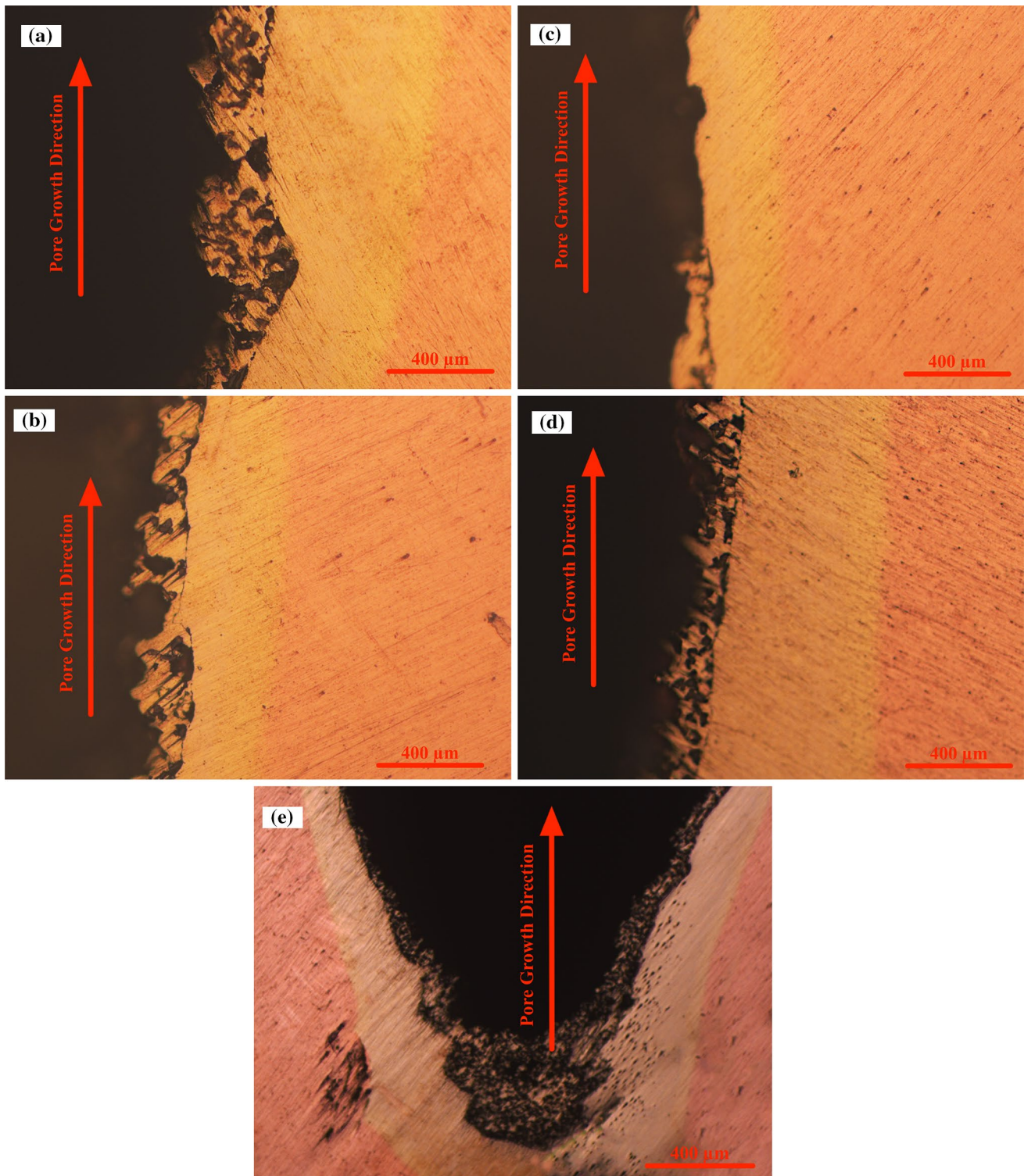
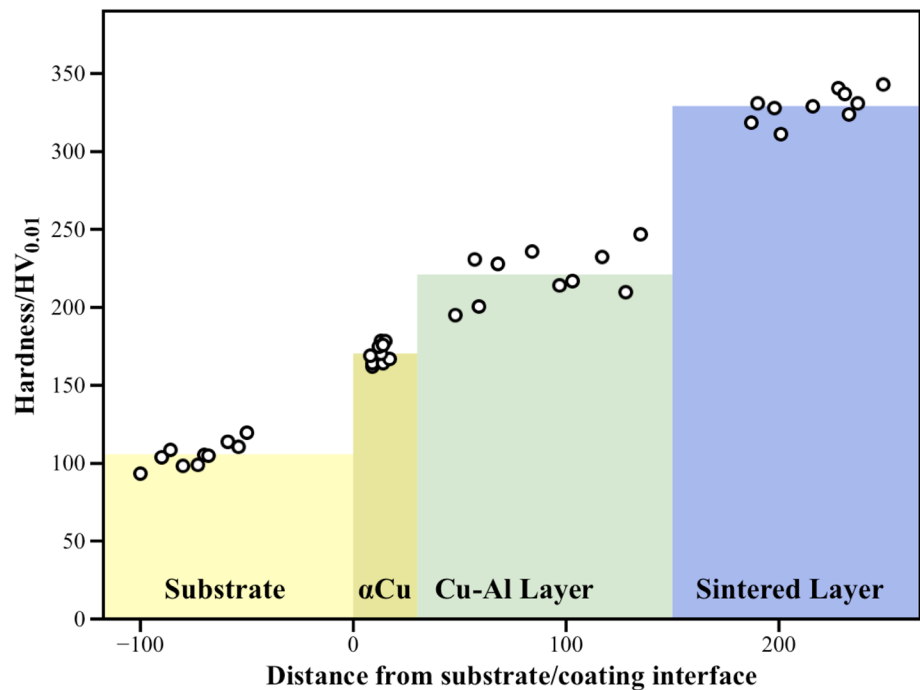


Fig. 5 Coating morphologies along the pore growth direction inside one pore at different depth: **a** near surface; **b** surface to middle; **c** middle to bottom; **d** near bottom; **e** bottom of a closed pore

Fig. 6 The hardness of Cu substrate and different parts of the coating



3.3 The hardness, the sliding property and the wear rate

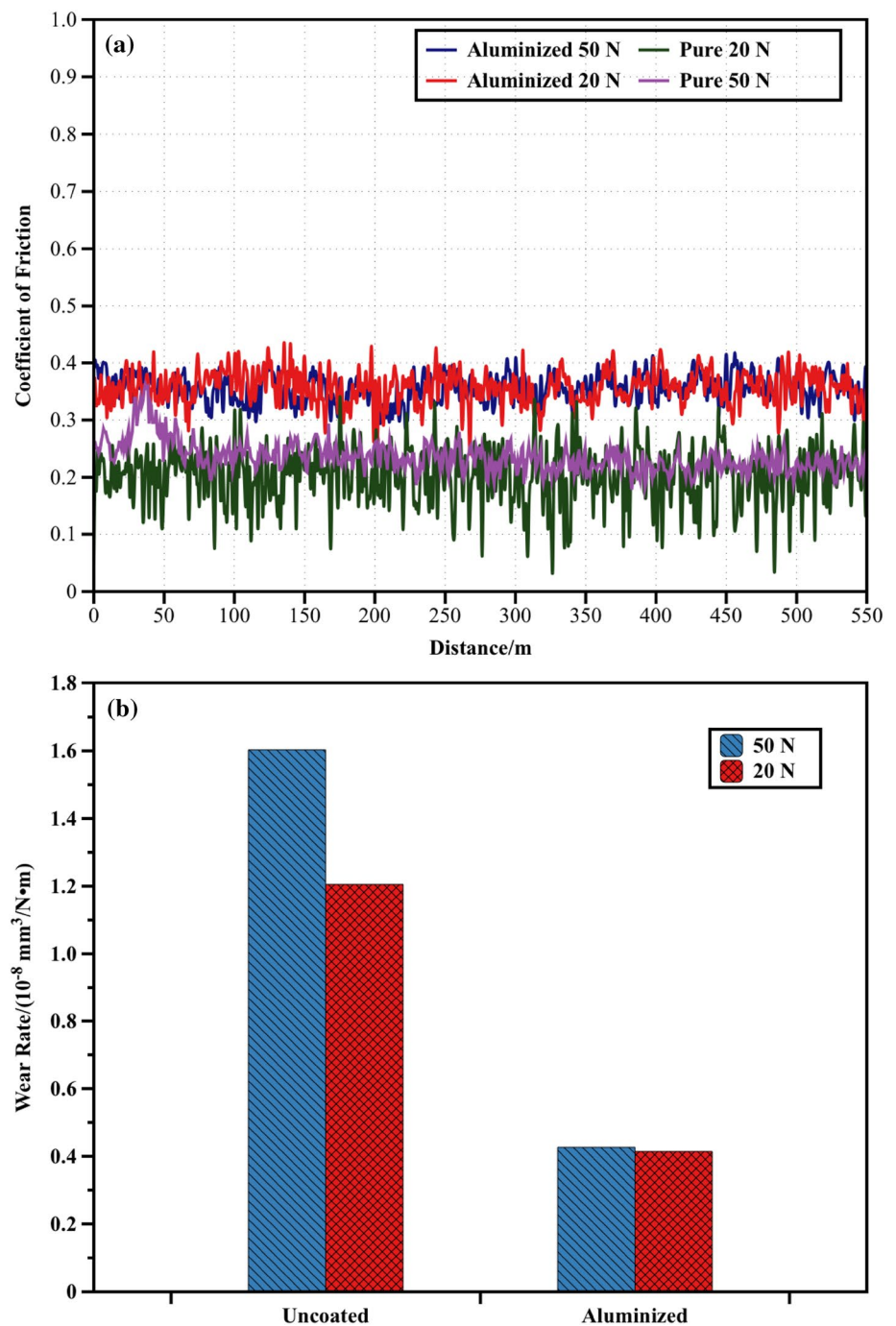
Figure 6 shows the hardness profile from the coatings to the Cu substrate, which is in accordance with the phase distribution in the aluminized coating mentioned above. The hardest part is the outermost layer, which is made of Al incorporating Al_2O_3 particles, being $300 \text{ HV}_{0.01}$, $70 \text{ HV}_{0.01}$ higher than that of the second layer, which corresponds to the Cu_3Al and Cu_9Al_4 layer, and three times as that of Cu substrate. Being the second soft phase in this system, the $\alpha\text{-Cu}$ with thickness of $20 \mu\text{m}$ on the substrate is still $70 \text{ HV}_{0.01}$ harder than that of copper. The aluminized coating has improved the hardness of the lotus-type porous copper significantly. It is expected that the increased hardness is beneficial to the improvement for the lotus-type porous copper on wear resistance, as well as the gradual hardness distribution for the stress relief which results in an enhancement on good adhesion between coating and substrate.

The comparison between uncoated and aluminized porous copper rings on coefficient of friction under the loads of 20 N and 50 N is shown in Fig. 7a. Neither the uncoated nor the aluminized copper ring has achieved smooth coefficient of friction curve during the process. The fluctuation is larger when the load is smaller, especially on the uncoated copper ring. The coefficient of friction of the aluminized copper is nearly twice as that of the uncoated one, while the wear rate of the aluminized copper is one quarter of that of the uncoated ones, as shown

in Fig. 7b. It is interesting to note that the wear rate of the aluminized copper is independent from the applied load, whereas the wear rate of the uncoated copper increases 33% when the load increases from 20 to 50 N. The load effect on wear rate is similar to that on the hardness for the specimen, where the penetration depth of indent increased as the surface hardness decreased or the load increased. As the aluminized coating increases the hardness of the substrate copper, so the wear rate decreases to its half or 1/3 for the lotus-type porous copper. On the other hand, the penetration depth of the abrasive (sliding mate) is deeper as the load increases, subsequent resulting in a higher wear rate. In the case of the aluminized copper, the results show it is independent from the applied load, which is not clear at present.

To understand the improved wear performance of the aluminized porous copper as well as the load effect, the worn surfaces of both the uncoated and the aluminized copper were compared, as shown in Fig. 8. The worn surface of the uncoated porous copper under the load of 50 N exhibits adhesive wear (Fig. 8b) while the specimen under the load of 20 N is predominated by adhesive wear with furrows (Fig. 8a). On the other side, the aluminized copper rings, both under the load of 20 N and 50 N were worn out by the furrow wear as shown in Fig. 8c, d. The furrows in Fig. 8c, d are about the same size as tip of the Al_2O_3 powder displayed in Fig. 3c, indicating that some Al_2O_3 particles peeled off onto the sliding surfaces acting as debris which could decrease the contact area of the two sliding surfaces and cause fewer adhesion

Fig. 7 Sliding properties of uncoated and aluminized lotus-type porous copper under the loads of 50 N and 20 N: **a** variation of coefficient of friction of the lotus-type porous copper rings with sliding distance; **b** wear rates



and larger coefficient of friction. This behavior can be observed in Fig. 8e where the Al_2O_3 particles in the sintered layer on the pore wall get peeled off to cause large furrows on the surface. In addition, the elevated surface hardness by the coating also contributes to the low wear rate as it prevents the debris penetrate deeper into the surface thus reducing the mass loss. By the results mentioned above, the wear mechanism for the aluminized lotus-type porous copper is summarized and shown in a diagram, as shown in Fig. 9.

4 Conclusions

The aluminized coating was deposited on pore walls of lotus-type porous copper successfully. The structure of the coating was characterized including thickness and its relationship with pore size, the elements composition and the phase composition. The properties such as hardness, coefficient of friction and the wear rate were evaluated and analyzed. The results indicate that:

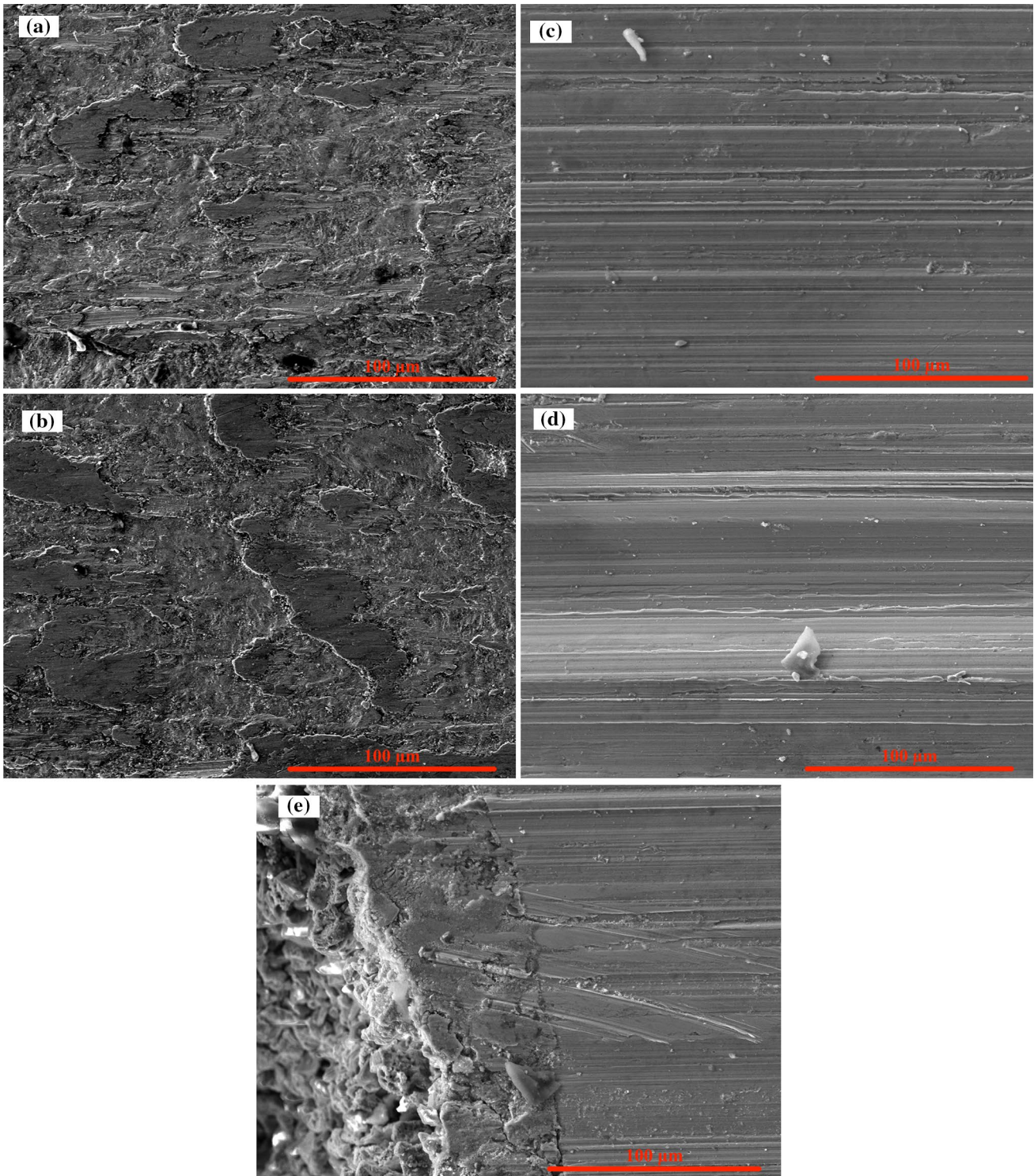


Fig. 8 Worn surfaces of the specimens: **a** uncoated 20 N; **b** uncoated 50 N; **c** aluminized 20 N; **d** aluminized 50 N; **e** aluminized under 50 N near the pore region

1. An aluminized coating can be achieved on the lotus-type porous copper with uniform thickness along the pores. The coating is consisted of two layers: an alloy layer which is made of two phases (α -Cu and the mixture of Cu_3Al and Cu_9Al_4) and a sintered layer where Al_2O_3 particles incorporated in Al substrate.
2. The thickness of the aluminized coating is strongly dependent on the pore size under the current experi-

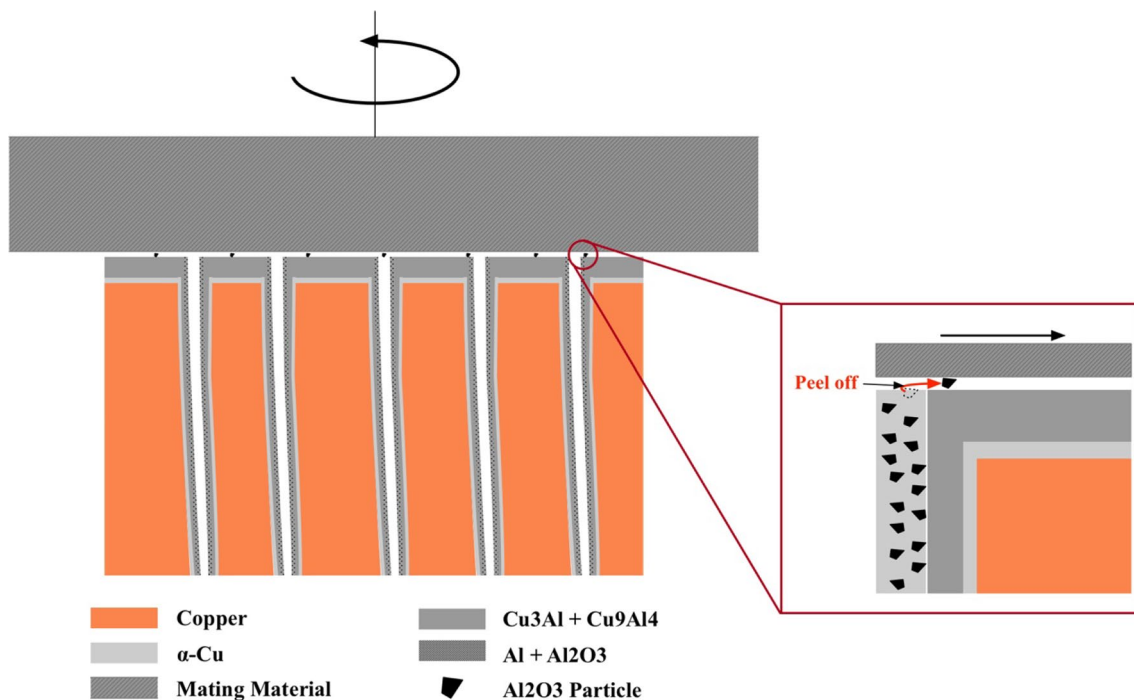


Fig. 9 Schematic of the sliding process on aluminized porous copper

ment condition: coatings on the larger pore are thicker than those on the smaller pore. It is hard to form an aluminized coating on the pores smaller than 300 μm in diameter. The relationship between the thickness and the pore size is not linear.

- The hardness is enhanced by a factor of three, which ranges from 105 to 302 $\text{HV}_{0.01}$ from copper substrate to the coating surface. Due to the shift from adhesion to furrow in wear mechanism caused by the coating, the wear resistance is improved by three quarters despite of the elevated coefficient of friction for the lotus-type porous copper.

Acknowledgements The financial support from Key state project of China (2017ZX02201001) is acknowledged.

Compliance with ethical standards

Conflict of interest The authors declare that they have no conflict of interest.

References

- Aoki T, Ikeda T, Nakajima H (2003) Fabrication of lotus-type porous brass by zinc diffusion into porous copper. *Mater Trans* 44:89–93
- Bansiddhi A, Sargeant TD, Stupp SI, Dunand DC (2008) Porous NiTi for bone implants: a review. *Acta Biomater* 4:773–782
- Batani MR, Ashrafizadeh F, Szpunar JA, Drew RAL (2002) Improving the tribological behavior of copper through novel Ti–Cu intermetallic coatings. *Wear* 253:626–639
- Boonyongmaneerat Y, Schuh CA, Dunand DC (2008) Mechanical properties of reticulated aluminum foams with electrodeposited Ni–W coatings. *Scr Mater* 59:336–339
- Chaliampalias D, Papazoglou M, Tsipas S, Pavlidou E, Skolianos S, Stergioudis G, Vourlias G (2010) The effect of Al and Cr additions on pack cementation zinc coatings. *Appl Surf Sci* 256:3618–3623
- Chiang KT, Kallenborn KJ, Yuen JL (1992) Aluminization of copper for oxidation protection. *Surf Coat Technol* 52:135–139
- Chiba H, Ogushi T, Nakajima H, Ikeda T (2004) Heat transfer capacity of lotus-type porous copper heat sink. *JSME Int J Ser B* 47:516–521
- Du H, Lu DZ, Qi JZ, Shen YF, Yin LS, Wang Y, Zheng ZG, Xiong TY (2014) Heat dissipation performance of porous copper with elongated cylindrical pores. *J Mater Sci Technol* 30:934–938
- Du H, Qi JZ, Du SQ, Xiong TY, Li TF, Lee SW (2010) Structure and oil retaining capacity of gasar copper fabricated by radial solidification with a combined crystallizer. *J Mater Process Technol* 210:1523–1528
- Du H, Qi JZ, Lao YX, Xiong TY (2012) Oil retaining capability and sliding friction behaviour of porous copper with elongated cylindrical pores. *J Mater Process Technol* 212:1796–1801
- Du H, Song GH, Nakajima H, Zhao YH, Xiao JQ, Xiong TY (2013) Study on lotus-type porous copper electroplated with a Ni coating on inner surface of pores. *Appl Surf Sci* 264:772–778
- Du M, Zhang HW, Li YX (2015) Inner surface alloying on pores of lotus-type porous copper through electroless plating with supersonic vibration and annealing treatment. *Surf Coat Technol* 261:1–6

13. Gu XN, Zhou WR, Zheng YF, Liu Y, Li YX (2010) Degradation and cytotoxicity of lotus-type porous pure magnesium as potential tissue engineering scaffold material. *Mater Lett* 64:1871–1874
14. Ikeda T, Nakajima H (2004) Titanium coating of lotus-type porous stainless steel by vapour deposition technique. *Mater Lett* 58:3807–3811
15. Li MY, Chao MJ, Liang EJ, Yu JM, Zhang JJ, Li DC (2011) Improving wear resistance of pure copper by laser surface modification. *Appl Surf Sci* 258:1599–1604
16. Liu J, Zhu X, Huang Z, Yu S, Yang X (2012) Characterization and property of microarc oxidation coatings on open-cell aluminum foams. *J Coat Technol Res* 9:357–363
17. Nakajima H (2007) Fabrication, properties and application of porous metals with directional pores. *Prog Mater Sci* 52:1091–1173
18. Ng KW, Man HC, Cheng FT, Yue TM (2007) Laser cladding of copper with molybdenum for wear resistance enhancement in electrical contacts. *Appl Surf Sci* 253:6236–6241
19. Ogushi T, Chiba H, Nakajima H (2006) Development of lotus-type porous copper heat sink. *Mater Trans* 47:2240–2247
20. Saeidi D, Alemrajabi AA, Saeidi N (2015) Experimental study of pool boiling characteristic of an aluminized copper surface. *Int J Heat Mass Transf* 85:239–246
21. Wang HX, Zhang Y, Cheng JL, Li YS (2015) High temperature oxidation resistance and microstructure change of aluminized coating on copper substrate. *Trans Nonferr Metal Soc* 25:184–190
22. Wei L, Hu X, Yu J, Huang Y (2014) Aluminizing and oxidation treatments on the porous stainless steel substrate for preparation of H₂-permeable composite palladium membranes. *Int J Hydrog Energy* 39:18618–18624
23. Xie Z, Tane M, Hyun SK, Okuda Y, Nakajima H (2006) Vibration-damping capacity of lotus-type porous magnesium. *Mater Sci Eng A* 417:129–133
24. Zhang HW, Chen LT, Liu Y, Li YX (2013) Experimental study on heat transfer performance of lotus-type porous copper heat sink. *Int J Heat Mass Transf* 56:172–180